POLITECNICO DI TORINO
Repository ISTITUZIONALE

Planning tools for next-generation DSP-based passive optical networks above 50G [Invited Tutorial]

Original
Planning tools for next-generation DSP-based passive optical networks above 50G [Invited Tutorial] / Rizzelli Martella, G., Gaudino, R.. - In: JOURNAL OF OPTICAL COMMUNICATIONS AND NETWORKING. - ISSN 1943-0620. - STAMPA. - 16:7(2024), pp. 88-96. [10.1364/JOCN.516669]

Availability:
This version is available at: 11583/2991972 since: 2024-11-07T09:41:34Z

Publisher:
Optica Publ. - IEEE

Published
DOI:10.1364/JOCN.516669

Terms of use:

This article is made available under terms and conditions as specified in the corresponding bibliographic description in the repository

Publisher copyright
Optica Publishing Group (formely OSA) postprint/Author's Accepted Manuscript

“© 2024 Optica Publishing Group. One print or electronic copy may be made for personal use only. Systematic reproduction and distribution, duplication of any material in this paper for a fee or for commercial purposes, or modifications of the content of this paper are prohibited.”

(Article begins on next page)

16 October 2026

Planning Tools for Next Generation DSP-based Passive Optical Networks above 50G
Invited/Tutorial paper

GIUSEPPE RIZZELLI[1,*] AND ROBERTO GAUDINO, *Senior Member, IEEE*[1]

[1] *Dipartimento di Elettronica e Telecomunicazioni (DET), Politecnico di Torino, Torino, Italy*
[*] *giuseppe.rizzelli@polito.it*

Compiled November 7, 2024

Next-generation optical access networks are evolving towards ultra-high bit rate (above 50 Gbps per wavelength) and extended fiber reach architectures. This trend will likely push the optoelectronics to their limits, thus requiring impairment compensation based on Digital Signal Processing (DSP) techniques in the transceivers. In this paper, which is an invited follow-up of a tutorial given at ECOC2023, we first present an overview of this evolving scenario and then we propose a unified analytical model that is able to predict the performance of these new systems for both direct-detection and coherent transceiver types. We believe that this model can be useful for preliminary scalability studies of new access architectures (as it happens in international standardization bodies). Moreover, when they are deployed, it can be useful as a base for network planning tools, particularly if future transceivers will be, as expected, highly re-configurable at the DSP level.

http://dx.doi.org/10.1364/ao.XX.XXXXXX

1. INTRODUCTION

Optical access networks for Fiber-to-the-Home (FTTH) using the Passive Optical Network (PON) architecture are today so widespread worldwide that they are expected to be continuously upgraded to higher bit rates. This will be demanded by the future use of PON for new trends such as industrial PON, Passive Optical LAN (POL), Fiber-to-the-Desk (FTTD) and, most important, mid-hauling or front-hauling for advanced 5G and future 6G mobile networks. This PON roadmap towards higher speed is evident by looking at the current evolution of PON standards in ITU-T [1, 2], which recently released ITU-T G.9804 50G-PON and is currently brainstorming in G.suppl.VHSP on the next steps above 50G-PON towards 100G-PON or 200G-PON. Whereas, in the commercial deployment, we are today seeing the first commercial installations of XG-PON and XGS-PON at 10 Gbps (after more than fifteen years dominated by GPON and EPON deployments).

Given the specific physical layer imposed by PON Optical Distribution Networks (ODN), such as the minimum 29 dB ODN loss necessary for class N1 PON, future upgrades to more than 50 Gbps per wavelength will require a significant technological evolution, as we discussed in the ECOC2023 tutorial [3] (by R. Gaudino) titled "Towards More and More DSP in Higher Speed PON" (the present paper is an invited follow-up of the ECOC2023 Tutorial). In particular, a significant evolution is required in terms of both higher bandwidth opto-electronics and Digital Signal Processing (DSP) additional functionalities in the transceivers to combat physical layer impairments. The recent literature and the discussion that is currently ongoing in ITU-T G.suppl.VHSP is proposing, among other issues, to add flexibility in the transceivers [4, 5] to evolve from the current "static" PON physical layer (i.e. fixed modulation format, bit rate, forward error correction (FEC) threshold etc.) to a more dynamic approach in which, thanks to the features offered by advanced DSP, the PON transceiver is set to a configuration which adaptively depends on the quality of the ODN on which it must operate and on the actual traffic requests. Moreover, some papers are also starting to propose the use of polarization multiplexed quadrature amplitude modulation (PM-QAM) coherent transmission in PON [6, 7] for higher bit rates and, if needed, for extended fiber reach architectures, like for the convergence between the metro and the access segments [8, 9].

If and when PON use a dynamic, DSP-based and adaptive physical layer, a proper set of software numerical models will be needed during the standardization phase to analyze the scalability of the proposed solutions, and then to real-time optimize the operation during the actual deployment. In this invited paper, we thus elaborate on these topics, by proposing two (closely related) analytical software models that are very effective in predicting the performance and then in dimensioning DSP-equalized intensity modulation and direct detection (IM-DD) high speed transmission [10] and coherent systems

[11] in the presence of strong optoelectronic bandwidth limitations, chromatic dispersion and the most relevant noise sources. Thanks to these two models, that are summarized in Appendixes A and B at the end of the paper, we can present a set of scalability studies for next generation PON networks, focusing on highest possible bit rates and, particularly for coherent solutions, extended fiber reach. In fact, this is the main novelty of this paper: while the two models were already presented in two previous papers of ours, here we extensively show how they can be effectively used in dimensioning next-generation ultra-high speed PON. Moreover, we further extend our models to include the effect of transmitter chirp (for IM-DD) and interference from backreflected counterpropagating signals (for coherent). The required central processing unit (CPU) time to run our model is extremely small since, as shown in Appendix A, it only requires as inputs spectrally-resolved transfer functions and power spectral densities (PSD) for the useful signal and for the noises, and it is then based on the computation of an integral of the resulting spectrally resolved signal-to-noise ratio $SNR(f)$. To give an idea, the CPU-time required on a standard desktop PC, with 4.8 GHz 12 core processor and 16 GB RAM memory, to generate the approx. 1000 BER values shown in the following Fig. 7 is about 2.8 seconds, i.e. 2.8 milliseconds for the estimation of each BER value. Thus, our models can potentially be used for the in-field optimization of the network in real-time and this demonstration is left for future study.

A specific feature of the proposed numerical modeling, thanks to its "spectrally resolved" approach, is its ability to take into account any bandwidth limitations induced by both optical and electrical filters. We believe that this feature will be increasingly relevant for next-generation ultra-high speed transceivers at speeds above 50 Gbaud (for both IM-DD and coherent cases) which, short of considerable advancements in device technologies will likely be operated in a strongly band-limited situation that will induce a high penalty (in received power and/or optical signal to noise ratio (OSNR) sensitiviy) that can be partially compensated by DSP functionalities and should be predicted in network planning tools.

Moreover, and for the coherent case, we believe that our proposal covers another current "gap" in today's coherent transceiver modeling, since it predicts receiver performance in any combination of optical amplified spontaneous emission (ASE) noise and receiver "electrical" noise, as it would happen for instance in the downstream direction of metro+PON converged architectures, where the metro segment adds ASE noise and, at the same time, the PON optical network unit (ONU) receiver is operated at very low received power.

Before proceeding with the "core" of our paper, we point out that the results presented in the following are obtained through the semi-analytical models that we proposed and validated against full numerical simulations and experiments in [10] and [11]. If the reader is not familiar with these models, we give a short summary in the two Appendixes at the end of the paper. Here we only remind that the proposed model for IM-DD can take into account all the most relevant noise sources, any linear transfer function for the electrical bandwidth limitations and the impact of chromatic dispersion and chirp (with a reasonable approximation). However, it cannot take into account in a "native" way nonlinear impairments due to the devices or the fiber propagation, even though some "ad hoc" extensions to account for weakly nonlinear propagation can be applied. The model for coherent detection, besides optical and electrical bandwidth limitations, can also deal with incoherent crosstalk due to ODN backreflections, any mix of electrical noises and optical noises (including the nonlinear Gaussian noise generated by Kerr effects in the fiber) and the impact of polarization-related impairments, such as polarization dependent loss in the reconfigurable optical Add-Drop Multiplexers (ROADMs). In both the IM-DD and coherent version the model cannot natively consider the impairments generated by burst-mode upstream transmission.

2. MODELING AND SCALABILITY OF DSP-BASED DIRECT-DETECTION PON

As discussed in details in many recent papers (such as [4] and [5]), IM-DD PON transmission above 50 Gbps per λ will be strongly limited by a combination of receiver noise, bandwidth limitation in the transceivers (both at the transmitter TX and at the receiver RX) and chromatic dispersion in the fiber. We showed and validated experimentally in [10] that the model summarized in Appendix A can predict the impact of all these impairments in a fairly large set of practical situations, with the only assumption that the receiver adaptive equalizer is sufficiently long to compensate for the end-to-end total impulse response of the system.

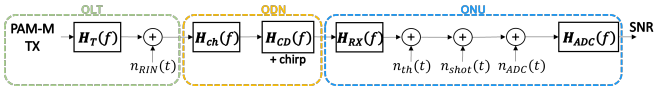

Fig. 1. Block diagram of the analytical model transfer functions and noise terms when applied to IM-DD.

Fig. 1 shows the schematic of the IM-DD PON that can be analyzed through our model, including the locations where noise contributions are added to the signal. $H_T(f)$, $H_{ch}(f)$, $H_{CD}(f)$, $H_{RX}(f)$ and $H_{ADC}(f)$ represent the transfer functions of the TX spectral shaping filter, the channel, the chromatic dispersion including chirp, the receiver and the analog to digital converter (ADC), respectively. $n_{RIN}(t)$, $= n_{th}(t)$, $n_{shot}(t)$ and $n_{ADC}(t)$ represent the individual contributions of the relative intensity noise (RIN), thermal, shot and ADC noise, respectively. In a first example of application, for a PON downstream transmission system, we investigate the impact of avalanche-photodiode (APD) available bandwidth BW_{APD} since it is today the optoelectronic element that is expected to be the main bottleneck in the evolution towards higher bit rate IM-DD PON. The APD parameters are taken from [12] as follows: gain $G = 8$ dB, excess noise factor $F = 3$ dB, responsivity $R = 0.8$ A/W, input referred noise density $IRND = 10\ pA/\sqrt{Hz}$. We also focus our attention on the bandwidth limitation and noise generated by the ADC that are needed in DSP-based receiver, since, as discussed in detail in [13], they are expected to present some scalability problem towards higher baud rate. Thus, all the results presented in the paper are obtained including the quantization noise and filtering effect associated with the ADC. Both ADC and APD are analytically described with supergaussian profiles, respectively with order 3 and 1 to reproduce what we measured in the lab as closely as possible.We consider two ADC cases using the parameters of the real time oscilloscope we have in our laboratory, a Tektronix DPO77002SX with $ENOB \simeq 5$ and 200 GS/s maximum sampling rate, used in all our experimental validations [10, 11]. In the first case we consider the oscilloscope analog bandwidth $BW_ADC = 33GHz$, whereas in a second case, for comparison we assume the ADC to have an ideally high bandwidth (numerically set in our studies to $BW_ADC = 200GHz$).

The ADC sampling rate is set to 200 GS/s, the highest provided by the oscilloscope, assuming the use of 2 samples per symbol at the highest 100 GBaud considered symbol rate. Other parameters used in the rest of the paper are as follows: transmitted signal power 11 dBm (typical maximum value used in PON [14] to prevent the onset of nonlinear effects during fiber propagation), extinction ratio ER=7 dB and square root raised cosine (SRRC) pulse shape with 0.2 roll-off factor.

The results are shown in Fig. 2 in terms of maximum achievable ODN loss, computed as the difference between the transmitted power and the sensitivity at the target $BER = 10^{-2}$, as a function of the APD 3dB bandwidth BW_{APD}. For PAM-2 at 100G (blue curves), it is clear that BW_{APD} strongly affects system performance, but also that BW_{ADC} is very relevant. In fact, the PAM-2 curve for the realistic case BW_{ADC}=33 GHz strongly differs from the one assuming an ideal ADC with $BW_{ADC} = 200$ GHz. For PAM-4 at 100G (i.e. at 50 Gbaud, red curves) the request on BW_{APD} is significantly smaller and there is no difference between the two assumed BW_{ADC} values. We also report in yellow the somehow extreme case of PAM-4 at 200G where it becomes even more evident that the bandwidth requirements on BW_{APD} and BW_{ADC} would become extremely tight. To summarize, Fig. 2 shows that modulation formats can provide 29 dB ODN loss (the minimum ODN loss class standardized by ITU-T) at 100 Gbps for APD bandwidth above 12 GHz and 23 GHz for PAM-4 and PAM-2 respectively, and there are margin for even higher ODN loss for larger available bandwidth. At 200 Gbps, on the other hand, a very high APD bandwidth in excess of 40 GHz is required for PAM-4 modulation with very large BW_{ADC}. This graph is a first example of how our proposed model can be very effective in a general design of the physical layers of future PON architectures.

In a second example of application, we show in Fig. 3 the impact of transmitter chirp and chromatic dispersion, by reporting again the maximum achievable ODN loss for a target BER=10^{-2} as a function of the accumulated dispersion $D \cdot L$ (in [ps/nm] and assuming O-band transmission), where D is the dispersion parameter and L is the fiber length, for different transmitter chirp [15] parameters α (inside the typical range for electro-absorption modulators (EAM) at the transmitter) and using PAM-4 100G transmission with BW_{APD}=13 GHz, which is the lowest possible value to obtain 29 dB ODN loss in the previous case shown in Fig. 2. To obtain this graph, we use the small-signal transfer function model for dispersion and chirp in IM-DD presented in [15]. The results shown in Fig. 3 highlight that only transmission close to the zero dispersion wavelength of the standard single mode fiber (SMF), in the O-band, can be allowed with 100G PAM-4 modulation. Thus, they can be useful to define the wavelength options (inside the O-Band) for future higher speed PON standards, also in relation to the expected zero-dispersion wavelength tolerances and on the expected chirp of the transmitter.

The results shown in the previous two Figures confirm that 100G-PON IM-DD downstream transmission is doable and can reach typical targets ODN loss (29+ dB or more) even using PAM-2, provided that a proper combination of optoelecronic bandwidth and dispersion/chirp values are selected. For what concerns 200G-PON, our analysis suggests that it would on the contrary be unfeasible on standard ODN loss classes. In fact, 200G transmission would be possible only on "non-standard" PON, such as for shorter distances and small splitting ratios (e.g. 1x4), a scenario that is sometimes considered in some of the proposed fronthauling architectures where the point-to-multipoint

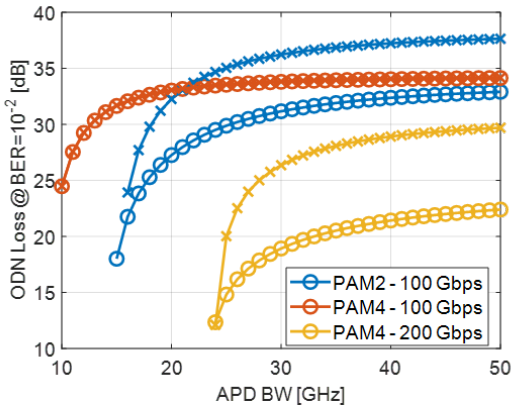

Fig. 2. ODN Loss at $BER = 10^{-2}$ vs. APD bandwidth BW_{APD}. The ADC bandwidth is 33 GHz (circles) or "unlimited" and actually set to 200 GHz (crosses).

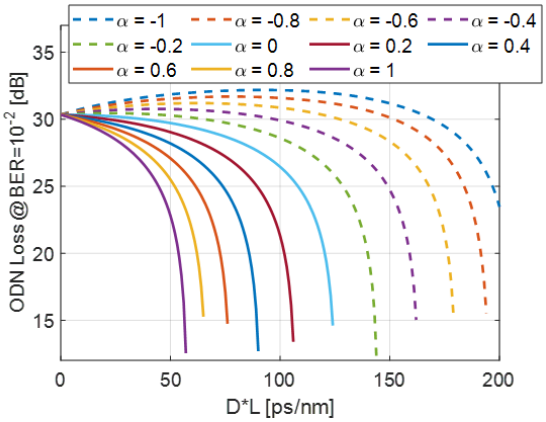

Fig. 3. ODN Loss at $BER = 10^{-2}$ vs. accumulated chromatic dispersion for several values of the EAM chirp α parameter for 100G-PON PAM-4. Dashed curves are for negative α. The baseline condition (no chirp, no dispersion) allowed about 30.3 dB ODN loss.

can be of practical interest even for a small number of ONUs per PON. For 200G-PON, we also show the dispersion/chirp study in Fig. 4, which points out that dispersion would become extremely critical even when working quite close to the zero dispersion wavelength in O-band. As an example, to have a small penalty in terms of ODN loss and on the curve for zero chirp ($\alpha = 0$) $D \cdot L$ should be below 20 ps/nm, requiring for a standard PON length of 20 km a dispersion value $D \leq 1$ ps/nm/km which would be extremely difficult to force due to the statistical variation of the SMF fiber zero dispersion wavelength.

3. MODELING AND SCALABILITY OF DSP-BASED COHERENT PON

By combining the models we proposed in [11, 16] and summarized in Appendix B, we can analyze a very wide range of coherent PON transmission scenarios. Fig. 5 shows the schematic of the coherent PON that can be analyzed through our model, including the locations where noise contributions are added to the signal. In addition to the IM-DD schematic, the coherent version includes also the contribution of the ASE noise $n_{ASE}(t)$ at the receiver input. Here we will focus on giving examples

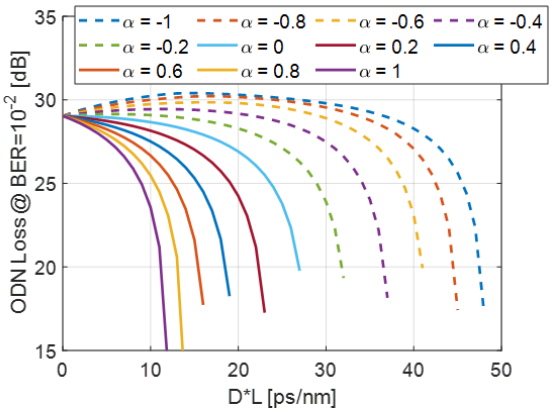

Fig. 4. ODN Loss at $BER = 10^{-2}$ vs. accumulated chromatic dispersion for several values of the EAM chirp α parameter for 200G-PON PAM-4. Dashed curves are for negative α. The baseline condition (no chirp, no dispersion, BW_{APD}=41 GHz, no ADC limitations) allowed about 29 dB ODN loss.

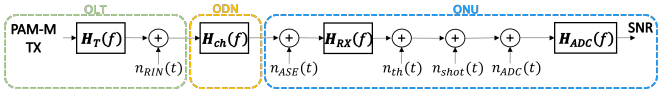

Fig. 5. Block diagram of the analytical model transfer functions and noise terms when applied to coherent communications.

for future higher bit rates, and in particular for 200G-PON and above, speeds that we proved in the previous Section to be hardly achievable with IM-DD. Moreover, we analyze future architectures such as the one shown in Fig. 6 where the metro and PON segments are merged, as we experimentally discussed in [8, 9], i.e. architectures where a given wavelength light-path is generated in the metro segment and then is optically amplified and filtered by (at least) one ROADM to be transparently routed on a standard PON (we discuss here the downstream DS direction but symmetrical considerations can be proposed for the upstream). In this scenario a tunable local oscillator is needed at the ONU to select the proper wavelength, as it is the case for current coherent transceivers. The rationale for analyzing this scenario is related to the idea that the somehow "giant" step of introducing PM-QAM coherent transmission also in PON could be techo-economically accepted in the future only if it enables not only higher bit rates compared to IM-DD but also significantly new network-level advantages. For instance, an optically-transparent converged metro-access architecture can allow the telco operators to reduce the number of central offices in large and dense cities. Moreover, due to the smaller amount of optical-to-electrical-to-optical (OEO) conversions, a converged metro-access architecture can potentially reduce the carbon-footprint of the network. However, these advantages will come at the cost of a much more complex network control plane which, in turn, will require physical-layer aware network planning tools also in the access network and not only, as it is the case today, in long-haul networks. We focus here on the current single wavelength solution and we analyze the single carrier and multicarrier implementation. However, the use of different wavelengths combined through a WDM filter is also being discussed.

We start by observing that a converged metro+PON transmission will ultimately be limited by a combination of the following impairments (the considerations are done here for the downstream direction):

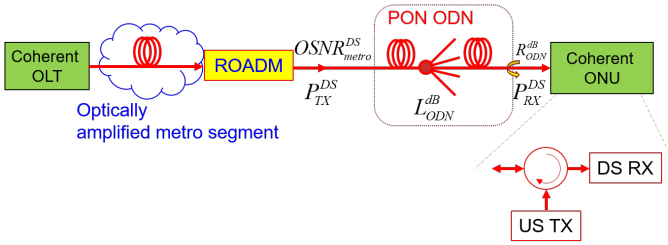

Fig. 6. Reference block diagram for the coherent metro+PON analysis, with main focus on DS direction.

- ASE noise introduced in the metro segment, resulting in a given OSNR at the metro output (indicated in Fig. 6 as $OSNR^{DS}_{metro}$); when relevant, $OSNR^{DS}_{metro}$ can include, beside ASE contributions, also equivalent Gaussian Noise (GN) generated by nonlinear effects in the fiber. In the rest of the paper, we use the convention of indicating OSNR with the noise measured on a bandwidth equal to 0.1 nm, unless otherwise explicitly noted;
- optical bandwidth limitations in the ROADMs, if any;
- electrical bandwidth limitations and electrical noises in the ONU coherent receiver; we note that the latter are typically very relevant since the ONU received power $P^{DS}_{RX,dBm} = P^{DS}_{TX,dBm} - L^{dB}_{ODN}$ is low for high target values of the ODN loss L^{dB}_{ODN}
- optical back-reflections in the ODN, determined by the ODN reflection R^{dB}_{ODN} (its value is, according to ODN ITU-T standards usually better than 32 dB in normal situations, but it can be as high as 20 dB for some specific ODN configurations, usually involving unterminated optical connectors)

In the following of this Section, we will investigate each of these effects. We start from the "baseline" situation of a PM-QAM transmission limited by ASE and coherent receiver noise while assuming all other physical layer parameters as ideal, showing in Fig. 7 the resulting BER vs. $P_{RX,dBm}$ for different values of $OSNR_{metro}$ (to avoid cumbersome mathematical notation we avoid from now on the "DS" apex in the formulae unless explicitly required), under the following assumptions: 50 GBaud PM-16QAM transmission (i.e. 400G-PON) with 0.7 A/W photodiode responsivity, $OSNR_{metro}$ ranging from 24 dB to 42 dB (using the aforementioned 0.1 nm convention) and with $N_0 = 2 \cdot 10^{-18}$ W^2/Hz the thermal noise PSD of the electrical part referred to the receiver input (thus including the insertion loss of the optical hybrid) and chosen to match the experimental sensitivity measurement [8].

We remind that the receiver sensitivity in terms of $P_{RX,dBm}$ is a key parameter for PON, since it will set the maximum achievable L^{dB}_{ODN} and thus the resulting PON ODN loss class. Fig. 7 shows that the dimensioning of the considered network will thus strongly depends on the available $OSNR^{DS}_{metro}$ at the metro output. For instance, under the above assumptions, $OSNR^{DS}_{metro}$ should be better than 32 dB to have a negligible reduction (<0.5 dB) on $P_{RX,dBm}$ sensitivity. To further elaborate on this point, we show in Fig. 8 the sensitivity $P_{RX,dBm}$ at $BER = 10^{-2}$ as a

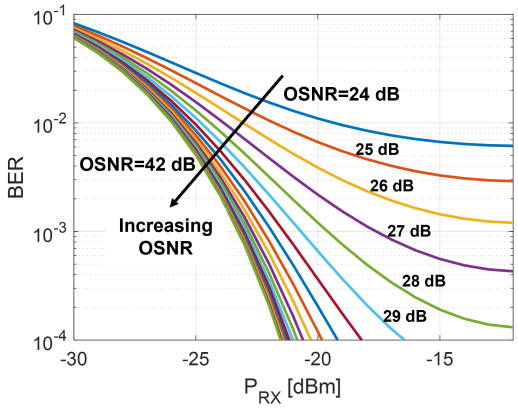

Fig. 7. Sensitivity curves for 50 GBaud PM-16QAM (i.e. 400G-PON) and several values of $OSNR_{metro}$ (defined on a 0.1 nm bandwidth) ranging from 24 dB to 42 dB with 1 dB step.

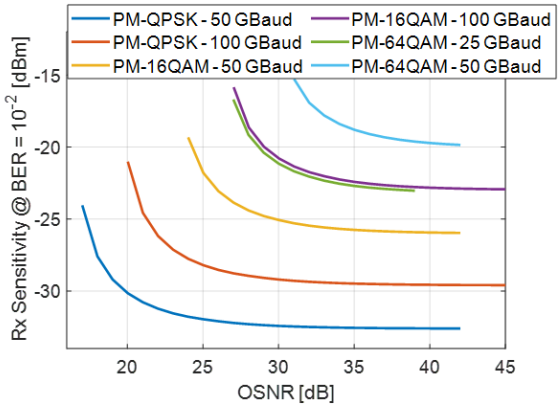

Fig. 8. Sensitivity at $BER = 10^{-2}$ vs. $OSNR_{metro}$ for different modulation formats and baud rates.

function of $OSNR^{DS}_{metro}$ for different baud rates and modulation formats.

The proposed model, thanks to its frequency-resolved approach, is also able to estimate the penalty introduced by any end-to-end linear transfer functions. As an example of this feature, we show in Fig. 9 the impact of different optical filtering bandwidth as plots of the achievable L^{dB}_{ODN} at $BER = 10^{-2}$ as a function of the $OSNR^{DS}_{metro}$ for 50 GBaud PM-16QAM (i.e. for 400G-PON) transmission with no receiver electrical filtering. The optical channel bandwidth is varied as a percentage of the symbol rate (the baseline condition for noise levels is the same as in the previous example). Similarly, we show in Fig. 10 the impact of electrical filtering bandwidth in the coherent transceivers in the same conditions as Fig. 9 with no optical channel filtering. Both the channel and the receiver transfer functions are described through a supergaussian filter, respectively with order 6 and 1.The system exhibit better tolerance to the electrical bandwidth limitation as in this case the ASE noise contribution is added before the receiver filtering stage. As discussed in [17], in fact, the impact of noise in a system with in-line filtering is maximum when the noise is added at the end of the communications link, after the filtering stages, as in the worst-case represented by the system with only optical filtering of Fig. 8, where ASE, shot and thermal noise are all inserted after the optical channel filtering stage.

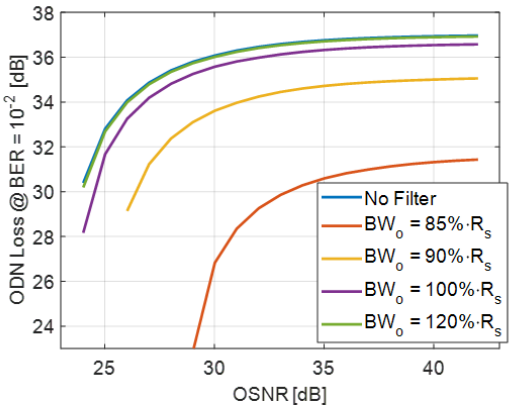

Fig. 9. ODN Loss at $BER = 10^{-2}$ for 50 GBaud PM-16QAM vs. $OSNR_{metro}$ for several values of the channel optical bandwidth as a percentage of the symbol rate.

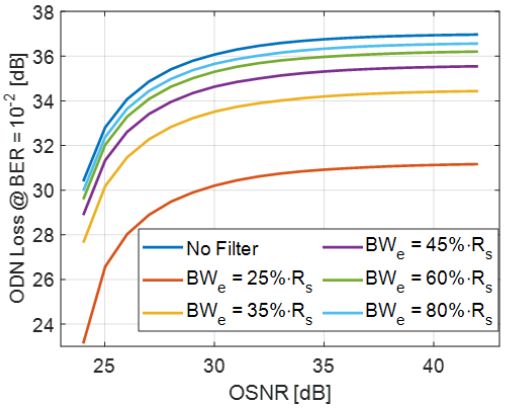

Fig. 10. ODN Loss at $BER = 10^{-2}$ for 50 GBaud PM-16QAM vs. $OSNR_{metro}$ for several values of the electrical transceiver bandwidth as a percentage of the symbol rate.

The set of graphs shown so far in this Section demonstrates that coherent transmission in metro+PON can reach very high values of L^{dB}_{ODN}. For instance, assuming $OSNR_{metro}$=25 dB and considering a DS transmitted power equal to 11 dBm, the achievable L^{dB}_{ODN} ranges from 43 dB at 200G using PM-QPSK modulation to 39 dB and 33 dB at 400G using PM-QPSK and PM-16QAM, respectively, which would then scale to smaller values if (optical or electrical) bandwidth limitations are present.

Anyway, for high ODN loss levels, optical back reflections become a very significant problems, since $P^{DS}_{RX,dBm}$ may become comparable with the ODN back-reflected US signal which, using the notation shown in Fig. 6, has a power level equal to $P^{US}_{TX,dBm} - R^{dB}_{ODN}$. We remind that in long-haul transmission, a coherent transceiver always uses the *same* wavelength for both directions, to reduce cost and also for wavelength routing reasons. However, while long haul transceivers are coupled to two fibers, PON is single fiber and thus, as a first consequence, a PON coherent transceiver should be equipped with a circulator, as shown in the inset of Fig. 6. More importantly, for a standard single-carrier single wavelength transceiver, the US back-reflected optical spectrum will be totally superimposed to the received DS one (and vice-versa at the OLT for the upstream receiver), thus generating a penalty due to coherent crosstalk. To analyze the impact of back-reflections, we will refer to the

qualitative optical spectral situation shown in Fig. 11 and we will show that back-reflections may become a key consideration in designing coherent ONUs and optical line terminals (OLTs). We studied its impact in Fig. 12 considering a back reflected signal levels R_{ODN} dB below the useful signal level, with the ADC effect and without any optical or electrical filtering in a 50 GBaud PM-16QAM system. The Figure shows that for a standard single-carrier single wavelength transceiver, the penalty in terms of achievable ODN losses would be very strong for the ITU-T typical specified value R^{dB}_{ODN}=32 dB, with about 7 dB reduction with respect to the case without backreflection interference. For the (even more critical) case with R^{dB}_{ODN}=20 dB (the aforementioned situation envisioned by ITU-T in case of un-terminated connectors) we could not show the resulting curve, since essentially the bidirectional system would go out of service.

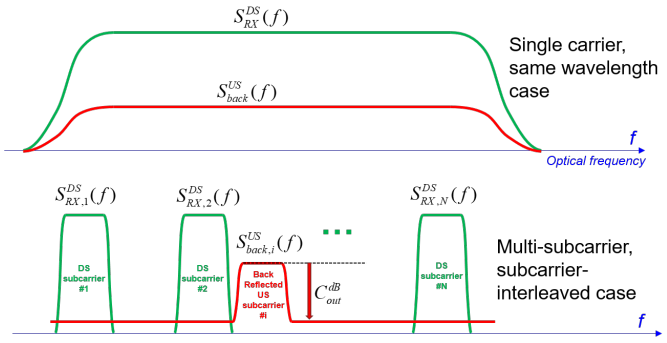

Fig. 11. Qualitative spectra for modeling backreflections levels.

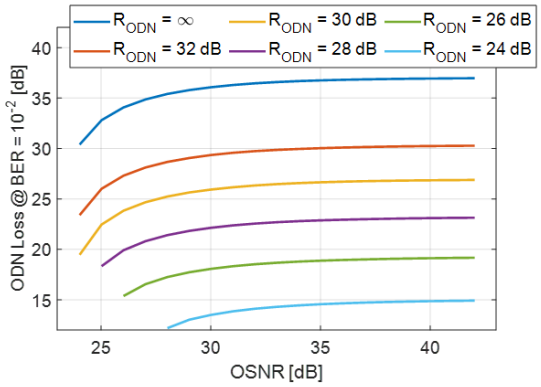

Fig. 12. ODN Loss at $BER = 10^{-2}$ for single-carrier same wavelength 50 GBaud PM-16QAM transmission vs. $OSNR_{metro}$ for several values of the backreflections level.

A significantly better situation in terms of back-reflections tolerance is possible when using the same wavelength with multi-subcarrier coherent transceivers (as proposed in [18, 19]) and alternating different optical subcarrier bands for the US and DS transmission, as already suggested in [20]. Assuming we have, both in US and DS, N=16 subcarriers at -1 dBm transmitted power, each PM-16QAM modulated at 4 Gbaud, for a total aggregated 64 GBaud symbol rate and 11 dBm optical power, we show the resulting performance for R^{dB}_{ODN}=20 dB in Fig. 13 and for R^{dB}_{ODN}=32 dB in Fig. 14 for different values of the "out-of-band" subcarrier spectral rejection C^{dB}_{out} (defined as shown in Fig. 11). The analysis is carried out considering a single backreflected subcarrier, the overall effect would thus depend on the number N of subcarriers.

In summary and regarding the impact of back-reflections, these last three figures show that single-carrier, same wavelength coherent transceivers would not be applicable to high ODN loss PON, so that if single-carrier transceivers are used, they must necessarily use two separate wavelengths for US and DS. For what concerns multi-subcarrier transceivers, the same wavelength and interleaved DS/US subcarrier scheme seems doable even at very high ODN loss, provided that the out-of-band subcarrier spectral rejection C^{dB}_{out} is sufficiently high.

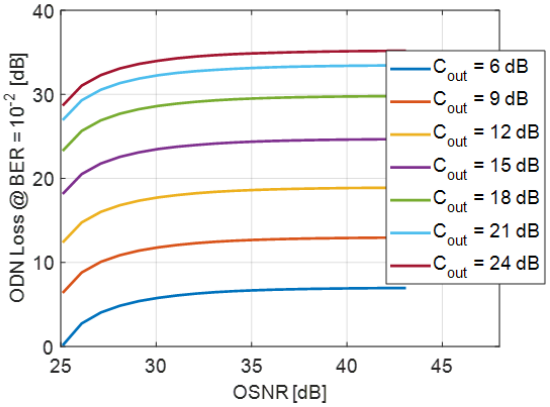

Fig. 13. ODN Loss at $BER = 10^{-2}$ for multi-subcarrier, same wavelength 50 GBaud PM-16QAM transmission vs. $OSNR_{metro}$ for several values of the C_{out} parameter when the backreflected signal is 20 dB below the transmitted one.

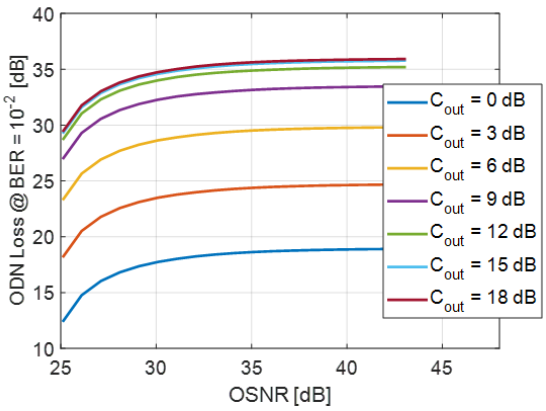

Fig. 14. ODN Loss at $BER = 10^{-2}$ for multi-subcarrier, same wavelength 50 GBaud PM-16QAM transmission vs. the $OSNR_{metro}$ for several values of the C_{out} parameter when the backreflected signal is 32 dB below the transmitted one.

4. CONCLUSION

We presented in this paper an analytical model for predicting the physical layer performance of next generation PON networks, showing its ability in considering a wide range of physical layer impairments (different type of noises, including quantization noise, optical and electrical filtering, back-reflections, etc.) under the assumption of a DSP-based receiver using a sufficiently long feed-forward adaptive equalizer. As we show in [10] a number of taps as low as 5 is sufficient to obtain less than 0.1 SNR estimation error with respect to full time domain simulations when

using FFE in a 56 GBaud PAM-4 transmission with strong bandwidth limitation, when the optical filter bandwidth is set at 25% of the symbol rate. This number does not seem critical as real implementations of the FFE equalizer make use of up to 20 taps. We then show examples of a wide range of applications for both IM-DD on a standard ODN PON and for coherent in an extended fiber reach configuration that may happen if and when metro and PON segments are optically merged. We believe that the model can be useful for two situations: feasibility and scalability studies for new access network architectures using extensions of the current PON paradigm, such as in standardization bodies for discussion on the so-called Physical Media Dependent (PMD) layer, and then, when a given network architecture is actually deployed, to use the models inside network planning tools, particularly if, as expected for the coherent case, the transceiver will have a quite large number of DSP-based reconfiguration options (at the very least baud rate and modulation format adapted to the specific link physical layer parameters).

Regarding the IM-DD model, we have shown here some specific scalability study examples, extending our previous work in [10]. We believe that the only important missing aspect for IM-DD is modeling the nonlinearities of the transceivers and of the fiber, a topic that anyway we believe may be addressed only on a case-by-case study, and not in a general modeling framework such as the one we tried to propose in this paper.

Regarding the coherent model, we also extended our previous work in [11], and we believe that our new proposal is quite complete, but that in future works it may be further improved in the following directions:

- if fiber nonlinearities are relevant, as in situations where DWDM is used in the metro segment, the well-established GN-model for fiber Kerr nonlinearities can be used, leading basically to another source of additive noise on top of the ASE term that we have already considered
- our model allows to consider any kind of electrical filtering, provided that it is identical on the four electrical paths (one for each of the four quadratures in PM-QAM) inside the coherent receiver. On the contrary, the model presented here cannot natively take into account asymmetric impairments in the receivers, such as different time-skews in the four electrical paths or the so-called I/Q imbalances and crosstalks, but we believe that it can be extended following the theory presented in [21]
- regarding alternative approaches for low cost coherent, such as Alamouti coding [22], we believe that our model con be properly extended to cope also with this variant, a task we will try to tackle in the near future.

5. APPENDIX A: THE FISCHER'S MODEL FOR IM-DD SYSTEMS

Our derivation of the IM-DD analytical model used in Section 2 is based on [23] and detailed in [10, 24]. Our original contribution to [23] stems from the fact that although thermal noise is typically signal independent, other noise sources such as relative intensity noise (RIN) and shot noise depend on the instantaneous signal power $P(t)$ (or $P(t)^2$ in the case of RIN). Moreover, bandwidth limitations due to optoelectronics components can be represented through linear frequency responses on $P(t)$.

Here we give a short summary of our previous contributions, which started from the model presented in [23] for a generic Bandlimited Additive Gaussian Noise (BAGN) channel, for which the Author presents an expression for the computation of the SNR at the output of an infinitely-long feed-forward equalizer (FFE) as follows:

$$SNR_{FFE} = \frac{1}{T \cdot \int_{-\frac{1}{2T}}^{\frac{1}{2T}} \frac{1}{\overline{SNR}(f)+1} df} - 1 \quad \textbf{(1)}$$

where T is the symbol period and $SNR(f)$ is the spectrally resolved SNR at the equalizer input, given by:

$$SNR(f) = \frac{T \cdot P_{TX} \cdot |H_T(f) \cdot H_{ch}(f)|^2}{N_0(f)} \quad \textbf{(2)}$$

where P_{TX} is the average transmitted signal power, $H_T(f)$ is the shaping filter frequency response at the transmitter, $H_{ch}(f)$ is the frequency response of the linear channel, and $N_0(f)$ is the power spectral density of the thermal noise at the input of the receiver.

In [10, 24] we eleborate on this BAGN model and made it applicable for an IM-DD optical channel using PAM-M modulation, obtaining the following expression:

$$S_{TX}(f) = \frac{T \cdot (OMA_{TX}^{outer})^2}{4 \cdot (M-1)^2} \cdot |H_T(f)|^2 \cdot \sigma_{\alpha_k}^2 \quad \textbf{(3)}$$

where α_k are the transmitted PAM-M intensity levels, $\sigma_{\alpha_k}^2 = \Sigma \alpha_k^2 / M$ and OMA_{TX}^{outer} is the PAM-M outer Optical Modulation Amplitude (OMA) in Watts. Fig. 1 shows the schematic of the IM-DD PON that can be analyzed through our model, including the locations where noise contributions are added to the signal. We can re-write equation 2 to include all the filtering effects and noise contributions, obtaining the general form:

$$SNR(f) = \frac{\sigma_{\alpha_k}^2}{4 \cdot (M-1)^2} \cdot \frac{T \cdot (OMA_{TX}^{outer})^2 \cdot |H_{Tot}(f)|^2}{S_N(f)} \quad \textbf{(4)}$$

where $|H_{Tot}(f)|^2 = |H_T(f)|^2 \cdot |H_{ch}(f)|^2 \cdot |H_{CD}(f)|^2 \cdot |H_{RX}(f)|^2 \cdot |H_{ADC}(f)|^2$ includes the cascade of all the possible filtering stages along the signal propagation path, namely the TX spectral shaping filter, the channel, the chromatic dispersion in a small signal approximation [15], the receiver (typically an APD in IM-DD systems) and the ADC. At the denominator of Eq. 4 $S_N(f) = S_{th}(f) + S_{RIN}(f) + S_{shot}(f) + S_{ADC}(f)$ represents the overall noise PSD as the sum of all the contributions, appropriately filtered:

- $S_{th}(f)$ is the PSD of the receiver additive thermal noise. It is white and added only at the ONU, before the ADC stage. It is not affected by the transmitted signal shape and it is filtered only by the ADC, thus $S_{th}(f) = N_0 \cdot |H_{ADC}(f)|^2$
- S_{RIN} is the PSD of the RIN noise that is filtered by $H_{Tot}(f)$, as the signal
- $S_{shot}(f)$ is the PSD of the shot noise, filtered only by the ADC, thus $S_{shot} = k_{shot} \cdot \overline{P_{RX}} \cdot |H_{ADC}(f)|^2$ where $\overline{P_{RX}}$ is the average received optical power and $k_{shot} = G^2 F q R^{-1}$ is a proportionality factor that depends on the photodetector excess noise figure F, the photodetector gain G (also called multiplication factor), the photodiode responsivity R and the electron charge q.
- $S_{ADC}(f)$ is the PSD of the quantization noise, which we modeled as proposed in [25] as a function of the ADC ENOB and signal peak-to-average power ratio (PAPR).

Finally, we showed in [10, 24] and validate it experimentally that the resulting SNR_{FFE} value can be inserted in the well-known erfc-like formula to obtain the resulting BER.

6. APPENDIX B: THE FISCHER'S MODEL FOR COHERENT SYSTEMS

The derivation of the analytical model used in Section 3 for optical coherent transmission is also based on [23] and detailed in [11]. Eqs. 1 and 2, properly modified, can also be used to compute the SNR at the FFE output in the case of coherent detection. In [11] we extended the work presented in [23] to address coherent communications in a generic polarization multiplexed scenario on a channel including frequency and polarization dependence on the signal and on the additive noise. Here, we further extend our model to include also the ADC and the associated quantization noise, optical amplification in order to study the impact of OSNR on the coherent system performance and the effect of optical back-reflections on the useful signal.

Using the same notation as in Appendix A and focusing on the polarization independent case, Eq. 4 in the coherent case becomes:

$$SNR(f) = \frac{P_{RX} \cdot |H_{Tot}(f)|^2}{R_S \cdot S_N(f) + S_{OSNR}(f) + S_{BR}(f)} \quad \textbf{(5)}$$

where $|H_{Tot}(f)|^2 = |H_T(f)|^2 \cdot |H_{ch}(f)|^2 \cdot |H_{RX}(f)|^2 \cdot |H_{ADC}(f)|^2$, R_S is the symbol rate, $S_N(f) = S_{th}(f) + S_{shot}(f) + S_{ADC}(f)$, $S_{OSNR}(f) = \frac{P_{RX}}{OSNR} \cdot |H_{RX}(f)|^2 \cdot |H_{ADC}(f)|^2$ is the PSD of the noise induced by the optical amplification with P_{RX} the received optical power and OSNR defined on bandwidth equal to the baud rate, and the PSD of the back-reflected interfering signal $S_{BR}(f)$ is again flat in the multi-subcarrier case and takes the same shape as the useful signal in the single carrier case as follows:

$$S_{BR}(f) = \frac{P_{TX} \cdot |H_T(f)|^2 \cdot |H_{RX}(f)|^2 \cdot |H_{ADC}(f)|^2}{R_{ODN} \cdot C_{out}} \quad \textbf{(6)}$$

R_{ODN} is the ODN reflection parameter and C_{out} is the "out-of-band" subcarrier spectral rejection parameter of the multi-subcarrier scenario (see Fig. 11).

ACKNOWLEDGMENT

The Authors would like to thank the European Union' Horizon Europe research and innovation programme, GA No. 101092766 (ALLEGRO) for funding this research. The experiments were carried out under the PhotoNext initiative at Politecnico di Torino. www.photonext.polito.it.

REFERENCES

1. J. S. Wey, "The Outlook for PON Standardization," *IEEE J. of Light. Techn.*, vol. 38, no. 1, pp. 31-42, Jan. 2020.
2. R. Bonk et al., "50G-PON: The First ITU-T Higher-Speed PON System," in IEEE Communications Magazine, vol. 60, no. 3, pp. 48-54, March 2022.
3. R. Gaudino, "Towards More and More DSP in Higher Speed PON", 2023 European Conference on Optical Communication (ECOC), 2023, doi: 10.5281/zenodo.10804307.
4. P. Torres-Ferrera, F. Effenberger, M. S. Faruk, S. J. Savory and R. Gaudino, "Overview of high-speed TDM-PON beyond 50 Gbps per wavelength using digital signal processing," in *Journal of Optical Communications and Networking*, vol. 14, no. 12, pp. 982-996, 2022.
5. R. Borkowski et al., "FLCS-PON – A 100 Gbit/s Flexible Passive Optical Network: Concepts and Field Trial," in *Journal of Lightwave Technology*, vol. 39, no. 16, pp. 5314-5324, Aug. 2021.
6. H. Zhang, Z. Jia, L. A. Campos and C. Knittle, "Low-Cost 100G Coherent PON Enabled by TFDM Digital Subchannels and Optical Injection Locking," 2023 Optical Fiber Communications Conference and Exhibition (OFC), San Diego, CA, USA, 2023, pp. 1-3, doi: 10.1364/OFC.2023.W1I.4.
7. T. Duthel et al., "DSP Design for Coherent Optical Point-to-Multipoint Transmission," in *Journal of Lightwave Technology*, vol. 42, no. 3, pp. 1109-1118, Feb. 2024.
8. G. Rizzelli et al., "Experimental Demonstration of In-Field 400G Coherent Metro-Access Convergence," in Optical Fiber Communications Conference and Exhibition (OFC) (2024), paper W1J.1.
9. M. Casasco et al., "Experimental Demonstration of a 400 Gb/s Full Coherent Transmission in an in-field Metro-Access scenario," 2023 23rd International Conference on Transparent Optical Networks (ICTON), Bucharest, Romania, 2023, pp. 1-4, doi: 10.1109/ICTON59386.2023.10207238.
10. G. Rizzelli, P. Torres-Ferrera, F. Forghieri and R. Gaudino, "An Analytical Model for Performance Estimation in Modern High-Capacity IMDD Systems," in *Journal of Lightwave Technology*, vol. 42, no. 5, pp. 1443-1452, March 2024.
11. G. Rizzelli, P. Torres-Ferrera and R. Gaudino, "An Analytical Model for Coherent Transmission Performance Estimation after Generic Jones Matrices," in *J. Light. Technol.*, vol. 41, no. 14, pp. 4582-4589, 2023.
12. R. Bonk et al., "Perspectives on and the road towards 100 Gb/s TDM PON with intensity-modulation and direct-detection," in *Journal of Optical Communications and Networking*, vol. 15, no. 8, pp. 518-526, August 2023.
13. P. J. Winzer, "The future of communications is massively parallel," in *Journal of Optical Communications and Networking*, vol. 15, no. 10, pp. 783-787, October 2023, doi: 10.1364/JOCN.496992.
14. "50-Gigabit-capable passive optical networks (50G-PON): Physical media dependent (PMD) layer specification," ITU-T G.9804.3.
15. L. Bjerkan, A. Royset, L. Hafskjaer and D. Myhre, "Measurement of laser parameters for simulation of high-speed fiberoptic systems," in *Journal of Lightwave Technology*, vol. 14, no. 5, pp. 839-850, May 1996, doi: 10.1109/50.495166.
16. G. Rizzelli, A. Nespola, S. Straullu, F. Forghieri and R. Gaudino, "Scaling Laws for Unamplified Coherent Transmission in Next-Generation Short-Reach and Access Networks," *J. Lightwave Technol.*, vol. 39, no. 18, pp.5805-5814, 2021.
17. I. F. de Jauregui Ruiz, A. Ghazisaeidi, T. Zami, S. Louis and B. Lavigne, "An accurate model for system performance analysis of optical fibre networks with in-line filtering," 45th European Conference on Optical Communication (ECOC 2019), Dublin, Ireland, 2019, pp. 1-4, doi: 10.1049/cp.2019.1112.
18. Welch, Dave, et al. "Point-to-multipoint optical networks using coherent digital subcarriers," in *Journal of Lightwave Technology*, vol.39, no. 16, pp. 5232-5247, 2021.
19. H. Zhang, Z. Jia, L. A. Campos and C. Knittle, "Rate-Flexible Coherent PON Up To 300 Gb/s Demonstrations with Low Complexity TDM Burst Design," 2023 Optical Fiber Communications Conference and Exhibition (OFC), San Diego, CA, USA, 2023, pp. 1-3, doi: 10.1364/OFC.2023.W1I.2.
20. P. Torres et al., "Single-Fiber Bidirectional Transmission using 400G Coherent Digital Subcarrier Transceivers," in Optical Fiber Communications Conference and Exhibition (OFC) (2024), paper Tu3E.5.
21. E. P. da Silva and D. Zibar, "Widely Linear Equalization for IQ Imbalance and Skew Compensation in Optical Coherent Receivers," in *Journal of Lightwave Technology*, vol. 34, no. 15, pp. 3577-3586, 1 Aug.1, 2016, doi: 10.1109/JLT.2016.2577716.
22. A. Hraghi, G. Rizzelli, A. Pagano, V. Ferrero, and R. Gaudino, "Analysis and experiments on C band 200G coherent PON based on Alamouti polarization-insensitive receivers," Opt. Express 30, 46782-46797 (2022).
23. Robert F.H. Fischer, "Linear Equalization," in *Precoding and Signal Shaping for Digital Transmission*, New York, NY, USA: Wiley-Interscience, 2002, ch. 2, sec. 2.2.4, pp. 35-43.
24. G. Rizzelli and R. Gaudino, "Analytical Performance Estimation Methods for Modern Optical Communications systems," 2023 Photonics Global Conference (PGC), Stockholm, Sweden, 2023, pp. 27-31.
25. A. Napoli et al., "Digital Compensation of Bandwidth Limitations for High-Speed DACs and ADCs," in *Journal of Lightwave Technology*, vol. 34, no. 13, pp. 3053-3064, July 2016.